J. Fluid Mech. (1986), *vol.* 169, *pp.* 109–123
Printed in Great Britain

On the origin of streamwise vortices in a turbulent boundary layer

By P. S. JANG,
Dynamics Technology, Inc., Torrance, CA 90503

D. J. BENNEY
Massachusetts Institute of Technology, Cambridge, MA 02139

AND R. L. GRAN
Dynamics Technology, Inc., Torrance, CA 90503

(Received 14 May 1985 and in revised form 9 September 1985)

Several experiments have suggested that streamwise vortices, with their accompanying low-momentum streaks in a turbulent boundary layer have a characteristic spanwise wavelength of approximately $\lambda_z^+ = 100$. Here a mechanism is proposed which selects a comparable spanwise wavelength and produces counter-rotating streamwise vortices in a turbulent boundary layer. Examining the equations which describe the deviation of the velocity field from its time-average, it is found that a resonance (Benney & Gustavsson 1981), is associated with the mean-velocity profile. As an integral part of this resonance, there is a mean secondary flow which has a spanwise wavelength $\lambda_z^+ = 90$ and whose velocities exhibit a streamwise vortex structure similar to those observed.

1. Introduction

During the last decade, much of the research on turbulent boundary layers has been concerned with the coherent eddy structures that have been observed near rigid boundaries. The quasi-deterministic, randomly located sequence of coherent structures, collectively called the bursting process, is believed to play a dominant role in the production and maintenance of a mean turbulent flow (for a review see Cantwell 1981).

One important aspect of the bursting process is believed to be the counter-rotating streamwise vortex structure with its accompanying low-speed streaks (for example, see Blackwelder 1979). From the many measurements of these streaks, it has been found that the mean streak spacing is approximately 100 ν/u_τ where u_τ is the friction velocity and ν is the kinematic viscosity. From flow visualizations, such as those by Kline *et al.* (1967), these low-speed streaks are usually observed to end by being lifted away from the wall. As they are lifted, the streaks start to oscillate with increasing amplitude leading to what is called breakdown. Corino & Brodkey (1969) showed that, soon after this breakdown, a large-scale motion emanating from the outer flow field approaches the wall and 'cleans' the entire region of the chaotic motion. This phase of the bursting process has been called the sweep.

In experiments using hot-wire anemometers, the bursting process is most easily characterized by a sharp acceleration of the streamwise velocity as reported by Wallace, Brodkey & Eckelmann (1977), and Blackwelder & Kaplan (1976). This

feature of the bursting process was used by Blackwelder & Kaplan as a detection technique to single out the bursting process from the chaotic turbulent motions. From conditional ensemble averages of data taken in such a way, Blackwelder suggested that the sharp acceleration is the transition between the low-speed streak and the sweep.

Recently, Blackwelder (1983) emphasized the similarity between the turbulent-boundary-layer bursting process and the transition problem. In particular, he found that the conditionally averaged streamwise velocity profile is highly inflexional at and before the burst detection. He further speculated that a localized shear-layer instability might play a role similar to that in the transition problem. The spatial scale of the oscillation of the lifted streak observed in the flow visualizations was noted to be consistent with such an interpretation. In any case, in Blackwelder's model, the counter-rotating streamwise vortex pair plays several important roles. The low-speed streaks are attributed to the vortex pair's 'pumping' action of the low-speed fluid away from the wall. In turn, the low-speed region is responsible (at least partially) for the inflexional velocity profile which eventually leads to breakdown through a shear-layer instability mechanism.

The aforementioned similarity between the bursting process and the transition problem has suggested to some that the streamwise vortices observed in either case might be due to the same mechanism. In this vein, Coles (1979), speculated that the streamwise vortices in a turbulent boundary layer might be the result of a Taylor–Görtler-type instability in which the concave flow is due to the large-scale motion in the outer flow field. This idea predicts a spanwise wavenumber for the vortex structure consistent with experiment. However, it appears difficult to justify the extension of the steady state Taylor–Görtler stability analysis to the unsteady flow field near the flat wall.

Benney (1961) and Lin & Benney (1962) proposed another mechanism which attributes the vortex structure in the transitional case to the secondary mean flow induced by the nonlinear interaction of a two- and a three-dimensional wave. Although this mechanism reproduced the essential features of Klebanoff, Tidstrom & Sargent's (1962) experiment it has been subject to some criticism. One of the weak points of the original theory is that the spanwise wavenumber of the three-dimensional wave was chosen to fit the experimental data rather than being predicted (see Stuart 1967). However, recent studies (Benney 1984) give theoretical justification for the approach.

The purpose of this paper is to provide a possible theoretical explanation for the appearance of streamwise vortices in a turbulent boundary layer. The present hypothesis stems from what is known as the direct-resonance concept introduced by Benney & Gustavsson (1981) in which a three-dimensional disturbance with certain wavenumbers can grow to a relatively large amplitude. Benney & Gustavsson showed that there exist exact resonances in various linearized laminar stability problems. However, they found that resonance conditions were only approximately satisfied for the case of Blausius flow. The effects of the resonance on the transition problem is therefore obscured by the existence of an unstable Tollmien–Schlichting wave and the fact that the resonance is only 'close'.

The turbulent-pipe-flow experiment by Morrison & Kronauer (1969) indicates that the statistically dominant streamwise fluctuations have a wavelike character. This suggests that a linear or weakly nonlinear perturbation analysis around the mean velocity might be applicable to the turbulent-boundary-layer problem. Along this line, Landahl (1967) and, subsequently, Bark (1975) examined the implications of the linear theory with given source terms coming from an assumed model for the

Reynolds stresses. A particularly interesting result is that Bark's computed energy spectrum for the streamwise velocity fluctuations displays preferred scales in the spanwise and streamwise directions and in time which are in good agreement with Morrison & Kronauer's measurements. However, the bandwidth of the computed spectrum is a few orders of magnitude smaller than was observed experimentally.

Bark attributed the sharpness of his computed spectrum to the crudeness of his model for the Reynolds stresses. However, his extremely sharp spectral peak suggests other possibilities such as some sort of resonance. Bark's method of solving the linearized equation for the vertical vorticity implicitly assumed that there is no resonance such as suggested by Benney & Gustavsson. This raises an interesting possibility that the Benney–Gustavsson resonance becomes exact if one replaces the Blasius profile with the mean turbulent profile. By examining the eigenvalues of the Orr–Sommerfeld problem and the vertical-vorticity equation, this was found to be the case. Details will be discussed in §2. Since this resonance becomes exact and since there is no unstable mode for the mean-velocity profile, the effects of the resonance could be more pronounced for the turbulent case than for the transition problem. Furthermore, the existence of this resonance offers a possible explanation for the observed scales in Morrison & Kronauer's experiment and the extreme sharpness of Bark's computed spectral peak.

Based upon direct resonance as an explanation for the preferred scales of the three-dimensional disturbances, we then examine the nonlinear effects of this resonance by using weakly nonlinear perturbation methods. It is shown in §3 that, as an integral part of this resonance, there is a mean secondary flow which has a spanwise wavelength 90 ν/u_τ and whose velocities exhibit counter-rotating streamwise vortex structures. There is some additional discussion in §4.

2. Direct resonance in a turbulent boundary layer

The velocity and pressure field in a turbulent boundary layer are split into three parts, following Reynolds & Hussain (1972):

$$U_i = \overline{u}_i + u_i + u_i', \tag{2.1}$$

$$P = \overline{p} + p + p', \tag{2.2}$$

where the overbar denotes the mean motion, the lower-case quantities, u_i and p, denote the wave-like motion periodic in the horizontal plane, and the prime denotes the turbulent motion. The equations governing the wave-like motion can be obtained by substituting (2.1) and (2.2) into the Navier–Stokes equations and subtracting the mean part from the phase averaged Navier–Stokes equations;

$$\frac{\partial u_i}{\partial t} + \overline{u}_j \nabla_j u_i + u_j \nabla_j \overline{u}_i = -\frac{1}{\rho}\nabla_i p + \nu \Delta u_i + \nabla_j(\overline{u_j u_i} - u_j u_i) - \nabla_j(\langle u_j' u_i' \rangle - \overline{u_j' u_i'}), \tag{2.3}$$

$$\nabla_i u_i = 0. \tag{2.4}$$

Here, $\langle\ \rangle$ denotes the phase averaging and ν is the kinematic viscosity, taken as constant.

The mean flow will be assumed to be parallel such that

$$\overline{u}_i = (\overline{u}(y), 0, 0). \tag{2.5}$$

The normal (y) coordinate dependence of $\overline{u}$ for the case of a turbulent boundary layer will be considered to be known. The key assumption in the analysis of (2.3) and (2.4)

is that the effects of the nonlinear terms in u_i are important only intermittently. The quasi-periodic streamwise vortices and the accompanying low-speed streaks, which seem to provide the set-up for a burst, are assumed to be weakly nonlinear phenomena.

Another assumption is that the effects of the last term of (2.3) are not important as far as the near-wall coherent structures are concerned. This assumption corresponds to the quasi-laminar model examined by Reynolds & Hussain. A partial justification for this assumption is that we found no substantial change in our results when the quasi-laminar model was replaced by the Newtonian eddy model (see Reynolds & Hussain, 1972).

On the basis of these assumptions, (2.3) and (2.4) are analysed using perturbation techniques. In the normal mode approach it is well known that all the eigenvalues of the linearized equations of (2.3) and (2.4) lead to decaying solutions, i.e. all disturbances lose energy to the mean flow. However, there is the possibility of a resonance by which disturbances with certain scales may grow, at least temporarily, by subtracting energy from the mean flow. Since the decay rates of eigenmodes whose peak values are near the turbulent boundary layer's sublayer are rather large, such a resonance will only be effective if it occurs in the lowest possible order of the expansion in order to reverse the energy loss even momentarily.

The direct resonance suggested by Benney & Gustavsson does arise in the linearized equations of (2.3) and (2.4). A particularly interesting property of the direct resonance is that, at a given Reynolds number, it occurs only at discrete locations in wavenumber space (i.e. only those components with certain combinations of wavelength and obliqueness are resonant). Therefore, this resonance appears to be an ideal candidate for it provides a mechanism which allows disturbances with only certain scales to dominate the dynamics.

To examine the possibility of direct resonance in a turbulent boundary layer, we utilize the boundary-layer displacement thickness δ^*, and the free-stream velocity $\overline{u}_\infty$ to non-dimensionalize the equations and set $\overline{u}_\infty \delta^*/\nu = R_*$. As is customary for the boundary-layer problem, x, y and z are taken to denote the streamwise, the normal and the spanwise coordinates respectively. The velocity components will be denoted by u, v and w. Elimination of the pressure from (2.3) gives

$$\left(\frac{\partial}{\partial t}+\overline{u}\frac{\partial}{\partial x}\right)\Delta v-\overline{u}''\frac{\partial v}{\partial x}+\epsilon\left[\left(\frac{\partial^2}{\partial x^2}+\frac{\partial^2}{\partial z^2}\right)S_2-\frac{\partial^2 S_1}{\partial x\,\partial y}-\frac{\partial^2 S_3}{\partial z\,\partial y}\right]=\frac{1}{R_*}\Delta^2 v, \tag{2.6}$$

$$\left(\frac{\partial}{\partial t}+\overline{u}\frac{\partial}{\partial x}\right)\eta+\overline{u}'\frac{\partial v}{\partial z}+\epsilon\left[\frac{\partial S_1}{\partial z}-\frac{\partial S_3}{\partial x}\right]=\frac{1}{R_*}\Delta\eta. \tag{2.7}$$

Here the primes denote differentiation with respect to y, η is the vertical vorticity, ϵ is a nonlinear parameter related to the small amplitude of the fluctuations, and the S_j are defined by

$$S_1=\frac{\partial}{\partial x}(uu-\overline{uu})+\frac{\partial}{\partial y}(vu-\overline{vu})+\frac{\partial}{\partial z}(wu-\overline{wu}), \tag{2.8}$$

$$S_2=\frac{\partial}{\partial x}(uv-\overline{uv})+\frac{\partial}{\partial y}(vv-\overline{vv})+\frac{\partial}{\partial z}(wv-\overline{wv}), \tag{2.9}$$

$$S_3=\frac{\partial}{\partial x}(uw-u\overline{w})+\frac{\partial}{\partial y}(vw-\overline{vw})+\frac{\partial}{\partial z}(ww-\overline{ww}). \tag{2.10}$$

The horizontal components of the velocity perturbation are related to v and η by the equations

$$\frac{\partial u}{\partial x}+\frac{\partial w}{\partial z}=-\frac{\partial v}{\partial y}, \tag{2.11}$$

$$\frac{\partial u}{\partial z}-\frac{\partial w}{\partial x}=\eta. \tag{2.12}$$

To review the essential ideas of direct resonance, (2.6) and (2.7) are linearized and normal mode solutions of the form

$$v=\hat{v}(y)\,\mathrm{e}^{\mathrm{i}\alpha x+\mathrm{i}\beta z-\mathrm{i}\omega t}, \tag{2.13}$$

$$\eta=\hat{\eta}(y)\,\mathrm{e}^{\mathrm{i}\alpha x+\mathrm{i}\beta z-\mathrm{i}\omega t}, \tag{2.14}$$

are sought, where α and β are wavenumber components in the streamwise and spanwise directions and ω is the wave frequency. This procedure leads to the following equations:

$$\left[\mathrm{i}\alpha(\bar{u}-c)\left(\frac{\partial^2}{\partial y^2}-\alpha^2-\beta^2\right)-\mathrm{i}\alpha\bar{u}''-\frac{1}{R^*}\left(\frac{\partial^2}{\partial y^2}-\alpha^2-\beta^2\right)^2\right]\hat{v}=0, \tag{2.15}$$

$$\left[\mathrm{i}\alpha(\bar{u}-c)-\frac{1}{R_*}\left(\frac{\partial^2}{\partial y^2}-\alpha^2-\beta^2\right)\right]\hat{\eta}=-\mathrm{i}\beta\bar{u}'\hat{v}, \tag{2.16}$$

subject to the boundary conditions $\hat{v}=0$, $\mathrm{d}\hat{v}/\mathrm{d}y=0$, $\hat{\eta}=0$ at $y=0,\ \infty$. Here, c denotes the phase velocity defined by $c=\omega/\alpha$. Equation (2.15) is the Orr–Sommerfeld (O–S) equation, and (2.16) will be referred to as the vertical-vorticity (V–V) equation. The O–S eigenvalue problem leads to a set of eigenvalues

$$c=c(\alpha,\beta;R_*). \tag{2.17}$$

The V–V equation is usually solved as a forced response. This approach implicitly assumes that the eigenfrequencies of the O–S equation do not match any of the free-mode eigenfrequencies for the V–V equation; that is, the eigenfrequencies of the problem

$$\left[\mathrm{i}\alpha(\bar{u}-c)-\frac{1}{R_*}\left(\frac{\partial^2}{\partial y^2}-\alpha^2-\beta^2\right)\right]\hat{\eta}_{\mathrm{F}}=0;\quad \hat{\eta}_{\mathrm{F}}=0\quad \text{at } y=0,\ \infty. \tag{2.18}$$

Denoting the set of V–V free-mode eigenfrequencies by

$$c'=c'(\alpha,\beta;R_*), \tag{2.19}$$

the condition for direct resonance can be written as

$$c(\alpha,\beta;R_*)=c'(\alpha,\beta;R_*). \tag{2.20}$$

If such a resonance condition is satisfied, the solution to the V–V equation behaves as

$$\eta\sim at\hat{\eta}_{\mathrm{F}}(y)\,\mathrm{e}^{-\mathrm{i}\omega t+\mathrm{i}\alpha x+\mathrm{i}\beta z}, \tag{2.21}$$

while

$$v\sim\hat{v}(y)\,\mathrm{e}^{-\mathrm{i}\omega t-\mathrm{i}\alpha x+\mathrm{i}\beta z}. \tag{2.22}$$

Note that the secular solution for η initially grows linearly with time so that relatively large horizontal motions would be induced. Here, the parameter a which determines the initial growth rate of the secular term is given by

$$a=\frac{\beta\int_0^\infty\hat{\eta}_{\mathrm{F}}u'\hat{v}\,\mathrm{d}y}{\int_0^\infty\hat{\eta}_{\mathrm{F}}\hat{\eta}_{\mathrm{F}}\,\mathrm{d}y}. \tag{2.23}$$

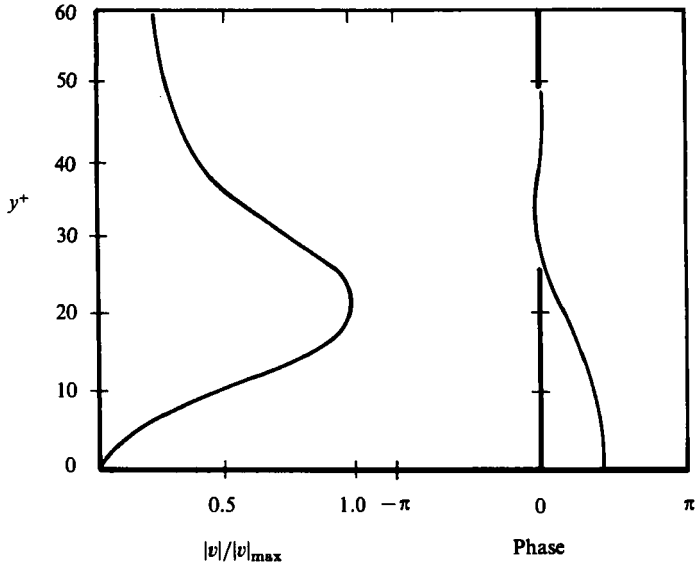

FIGURE 1. The amplitude and phase distribution of the resonant Orr–Sommerfeld mode.

In order to determine whether such a resonance occurs when $\overline{u}$ is taken to be a turbulent-boundary-layer mean profile, it is necessary to rely on numerical solutions of the eigenvalue problems associated with (2.15) and (2.18). If two eigenvalues coincide, then resonant growth occurs. One such resonance was found when the wavenumbers (expressed in 'wall units' $\alpha^+ \equiv \alpha\nu/u_\tau$) are

$$\alpha^+ = 0.0093, \tag{2.24}$$

$$\beta^+ = 0.035. \tag{2.25}$$

The location of this resonance in dimensionless wavenumber space appears to be relatively independent of the Reynolds number. (We examined the Reynolds-number dependence for the range $1000 \leqslant R_* \leqslant 15000$). At this resonant point the eigenfrequencies of the O–S and the V–V equations are the same and given by

$$\omega^+ \equiv \frac{\omega\nu}{u_\tau^2} = 0.090 - 0.037\mathrm{i}. \tag{2.26}$$

This resonance was found numerically by locating the intersection of the zero lines of the real and the imaginary parts of $[c(\alpha,\beta;R_*) - c'(\alpha,\beta;R_*)]$ in the (α,β)-plane. The boundary-layer velocity profile used for these computations incorporated the well-known law of the wall and law of the wake along with a sublayer 'patch' based on van Driest's damping factor. This sublayer patch results in a velocity profile that is in good agreement with experiment over the entire boundary layer. The normal coordinate dependence of the O–S eigenmode and V–V eigenmode are plotted in figures 1 and 2 respectively. No exhaustive numerical search was made for other resonances and while there may be some they will have higher damping rates.

If there is a potentially large amplitude associated with the secular behaviour, the above values of α^+, β^+ and ω_R^+ (real part of ω^+) should correspond to the position of a local peak in the power-spectral density of the horizontal velocity. Experimental evidence for the correctness of this prediction can be found in Morrison & Kronauer's (1969) experiment. Measuring the fluctuation of the streamwise velocity, they

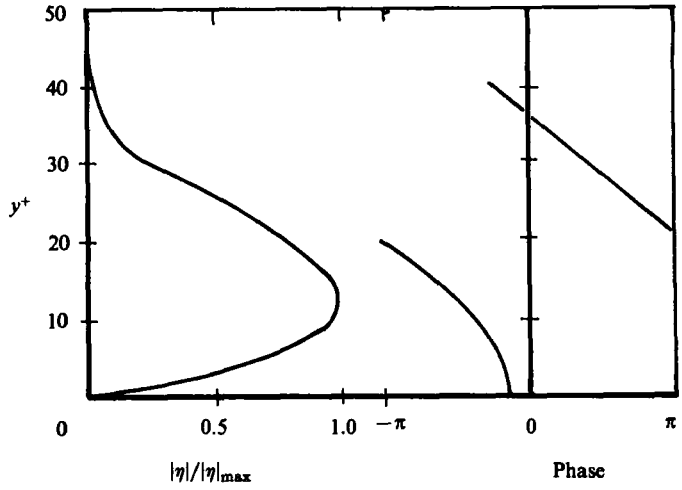

FIGURE 2. The amplitude and phase distribution of the resonant vertical-vorticity mode.

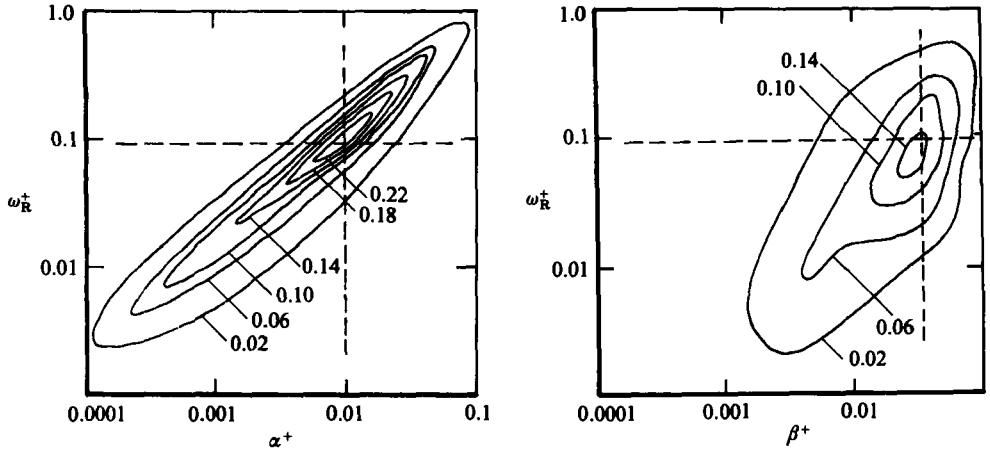

FIGURE 3. Comparison of the resonant point with the peak position of Morrison & Kronauer's spectrum.

obtained the power-spectral density as a function of ω_R and either α or β. Figure 3 shows their contour plots of $\mathscr{P}_{1u}(\alpha^+, \omega_R^+)$ and $\mathscr{P}_{2u}(\beta^+, \omega_R^+)$ where these quantities are related to the power spectrum P_u as

$$\mathscr{P}_{1u}(\alpha^+, \omega_R^+) = \alpha^+ \omega_R^+ \int_0^\infty P_u(\alpha^+, \beta^+, \omega_R^+)\, \mathrm{d}\beta^+, \tag{2.27}$$

$$\mathscr{P}_{2u}(\beta^+, \omega_R^+) = \beta^+ w_R^+ \int_0^\infty P_u(\alpha^+, \beta^+, \omega_R^+)\, \mathrm{d}\alpha^+. \tag{2.28}$$

These spectral functions plotted in log coordinates permit one to make a visual comparison of the relative power in various wavenumber/frequency bands (the power is the contour level times the area as seen in the figure).

The particular spectrum measured at $y^+ = 14.8$ was chosen because this location is the closest of Morrison & Kronauer's data to the peak of the resonant free mode

of the vertical-vorticity equation (see figure 2). The predicted position of the spectral peak based on the direct resonance is denoted in figure 3 by the intersection of the two dashed lines in each figure. The prediction is in good agreement with the experimental data.

3. Mean flow induced by the resonating fundamental modes

From (2.15) and (2.16), it is apparent that if α, β and ω correspond to a direct resonance, then so do α, $-\beta$ and ω. So, there are at least two resonant modes. The nonlinear theoretical consequences of two or more resonant modes were analysed by Benney & Gustavsson (1981). We shall rely on their formalism to compute the mean flow induced by these resonant modes.

They first observed that (2.6) and (2.7) imply that, for the case of two resonant modes, the dominant terms in the higher-order expansion for v and η are of the form

$$v \sim (1+\epsilon^2 t^4+\ldots)\,\mathrm{e}^{\mathrm{i}\alpha x+\mathrm{i}\beta z-\mathrm{i}\omega t}, \tag{3.1}$$

$$\eta \sim (t+\epsilon^2 t^5+\ldots)\,\mathrm{e}^{\mathrm{i}\alpha x+\mathrm{i}\beta z-\mathrm{i}\omega t}, \tag{3.2}$$

where ϵ is the nonlinear parameter related to the small amplitude of fluctuation. They argued that for imaginary part of ω sufficiently small, the appropriate timescale is $t\epsilon^{\frac{1}{2}}$ and the perturbation expansion must be rescaled in the form

$$v = V, \quad (u, w, \eta) = \epsilon^{-\frac{1}{2}}(U, W, N). \tag{3.3}$$

The nonlinear perturbation equations then become

$$\begin{aligned}\left[\left\{\left(\frac{\partial}{\partial t}+\overline{u}\frac{\partial}{\partial x}\right)\Delta-\overline{u}''\frac{\partial}{\partial x}-\frac{1}{R_*}\Delta^2\right\}V\right.&\\ \left.-\frac{\partial^3}{\partial x^2\,\partial y}(UU-\overline{UU})-2\frac{\partial^3}{\partial x\,\partial z\,\partial y}(UW-\overline{UW})-\frac{\partial^3}{\partial z^2\,\partial y}(WW-\overline{WW})\right]&\\ +\epsilon^{\frac{1}{2}}\left[\left(\frac{\partial^2}{\partial x^2}+\frac{\partial^2}{\partial z^2}-\frac{\partial^2}{\partial y^2}\right)\left(\frac{\partial}{\partial x}(UV-\overline{UV})+\frac{\partial}{\partial z}(WV-\overline{WV})\right)\right]&\\ +\epsilon\left[\left(\frac{\partial^2}{\partial x^2}+\frac{\partial^2}{\partial z^2}\right)\frac{\partial}{\partial y}(VV-\overline{VV})\right]=0,&\end{aligned} \tag{3.4}$$

$$\begin{aligned}\left[\left(\frac{\partial}{\partial t}+\overline{u}\frac{\partial}{\partial x}\right)-\frac{1}{R_*}\Delta\right]N+\epsilon^{\frac{1}{2}}\left[\overline{u}'\frac{\partial V}{\partial z}+\frac{\partial^2}{\partial x\,\partial z}\left((UU-\overline{UU})-(WW-\overline{WW})\right)\right.&\\ \left.+\left(\frac{\partial^2}{\partial z^2}-\frac{\partial^2}{\partial x^2}\right)(UW-\overline{UW})\right]+\epsilon\left[\frac{\partial^2}{\partial y\,\partial z}(UV-\overline{UV})-\frac{\partial^2}{\partial x\,\partial y}(VW-\overline{VW})\right]=0,&\end{aligned} \tag{3.5}$$

$$\frac{\partial U}{\partial x}+\frac{\partial W}{\partial z}+\epsilon^{\frac{1}{2}}\frac{\partial V}{\partial y}=0, \tag{3.6}$$

$$N=\frac{\partial U}{\partial z}-\frac{\partial W}{\partial x}. \tag{3.7}$$

Equation (3.5) is linear when $\epsilon = 0$, and a systematic perturbation scheme is readily developed (i.e. $N = N^{(0)}+\epsilon^{\frac{1}{2}}N^{(\frac{1}{2})}+\ldots$, etc.). The zeroth-order term in such an expansion gives

$$N^{(0)} = B\hat{\eta}_0(y)\sin\beta_0 z\,\mathrm{e}^{\mathrm{i}\alpha_0 x-\mathrm{i}\omega_0 t}+B^*\hat{\eta}_0^*(y)\sin\beta_0 z\,\mathrm{e}^{-\mathrm{i}\alpha_0 x+\mathrm{i}\omega_0 t}, \tag{3.8}$$

where * denotes the complex-conjugate. Note that the spanwise standing wave is taken as the solution since each of the resonances, ($\alpha = \alpha_0$, $\beta = \pm\beta_0$), are equally likely to occur. The function $\hat{\eta}_0$ is determined as a solution to the eigenvalue problem

$$\left[\mathrm{i}\alpha_0(\bar{u}-c)-\frac{1}{R_*}\left(\frac{\partial^2}{\partial y^2}-\alpha_0^2-\beta_0^2\right)\right]\hat{\eta}_0 = 0; \quad \hat{\eta}_0(0) = \hat{\eta}_0(\infty) = 0, \tag{3.9}$$

where α_0 and β_0 are the wavenumbers at the direct resonance. Using the continuity equation and the definition of N, $U^{(0)}$ and $W^{(0)}$ can be obtained from $N^{(0)}$ as

$$\begin{Bmatrix} U^{(0)} \\ W^{(0)} \end{Bmatrix} = B \begin{Bmatrix} -\dfrac{\beta_0\hat{\eta}_0}{\alpha_0^2+\beta_0^2}\cos\beta_0 z \\ \dfrac{\mathrm{i}\alpha_0\hat{\eta}_0}{\alpha_0^2+\beta_0^2}\sin\beta_0 z \end{Bmatrix} \mathrm{e}^{\mathrm{i}\alpha_0 x-\mathrm{i}\omega_0 t}+(*). \tag{3.10}$$

The equation for $V^{(0)}$ is obtained from (3.4):

$$\left\{\left(\frac{\partial}{\partial t}+\bar{u}\frac{\partial}{\partial x}\right)\Delta-\bar{u}''\frac{\partial}{\partial x}-\frac{1}{R_*}\Delta^2\right\}V^{(0)} = \frac{\partial^3}{\partial x^2\,\partial y}(U^{(0)}U^{(0)}) + 2\frac{\partial^3}{\partial x\,\partial z\,\partial y}(U^{(0)}W^{(0)})+\frac{\partial^3}{\partial z^2\,\partial y}(W^{(0)}W^{(0)}). \tag{3.11}$$

The time averages of $U^{(0)}U^{(0)}$, $U^{(0)}W^{(0)}$ and $W^{(0)}W^{(0)}$ are dropped since $U^{(0)}$ and $W^{(0)}$ eventually decay exponentially in time. An examination of the source terms shows that the particular solution for $V^{(0)}$ is of the form

$$V^{(0)} = V_{\mathrm{M}}(y,t)\cos(2\beta_0 z)+(V_{02}(y)\,e^{2\mathrm{i}\alpha_0 x-2\mathrm{i}\omega_0 t}+*). \tag{3.12}$$

We shall refer to the first term as the induced mean flow and the second term as the induced second harmonic. The function $V_{\mathrm{M}}(y,t)$ is determined as a solution of the following equation

$$\left[\frac{\partial}{\partial t}\left(\frac{\partial^2}{\partial y^2}-4\beta_0^2\right)-\frac{1}{R_*}\left(\frac{\partial^2}{\partial y^2}-4\beta_0^2\right)^2\right]V_{\mathrm{M}} = 4BB^*\frac{\alpha_0^2\beta_0^2}{(\alpha_0^2+\beta_0^2)^2}\frac{\partial(\hat{\eta}_0\hat{\eta}_0^*)}{\partial y}\mathrm{e}^{2\omega_{\mathrm{I}}t} \tag{3.13}$$

where ω_{I} is the imaginary part of ω_0. The function $V_{02}(y)$ is determined from

$$\left[(-2\mathrm{i}\omega_0+2\mathrm{i}\alpha_0\bar{u})\left(\frac{\partial^2}{\partial y^2}-4\alpha_0^2\right)-2\mathrm{i}\alpha_0\bar{u}''-\frac{1}{R_*}\left(\frac{\partial^2}{\partial y^2}-4\alpha_0^2\right)^2\right]V_{02} = -2B^2\frac{\alpha_0^2\beta_0^2}{(\alpha_0^2+\beta_0^2)^2}\frac{\partial(\hat{\eta}_0\hat{\eta}_0)}{\partial y}. \tag{3.14}$$

As long as $(2\omega_0)$ is not an eigenfrequency of the O–S problem for the case of $\alpha = 2\alpha_0$ and $\beta = 0$, the above equation for V_{02} has a solution.

However, the equation for the induced mean flow requires special treatment. Although the source term in the equation for V_{M} decays with time as $\exp(2\omega_{\mathrm{I}}t)$, the solution V_{M} cannot have the same time dependence. To illustrate this we first assume that V_{M} has the same exponential time dependence, in which case (3.13) reduces to

$$\left[2\omega_{\mathrm{I}}\left(\frac{\partial^2}{\partial y^2}-4\beta_0^2\right)-\frac{1}{R_*}\left(\frac{\partial^2}{\partial y^2}-4\beta_0^2\right)^2\right]\hat{V}_{\mathrm{M}} = 4BB^*\frac{\alpha_0^2\beta_0^2}{(\alpha_0^2+\beta_0^2)^2}\frac{\partial(\hat{\eta}_0\hat{\eta}_0^*)}{\partial y}, \tag{3.15}$$

where $\hat{V}_{\mathrm{M}}$ is defined by $V_{\mathrm{M}} = \hat{V}_{\mathrm{M}}(y)\,\mathrm{e}^{2\omega_{\mathrm{I}}t}$. For simplicity we assume that the right-hand side of the above equation vanishes for larger values of y. The asymptotic solution for $\hat{V}_{\mathrm{M}}$ will then be of the form

$$\hat{V}_{\mathrm{M}} = a\,\mathrm{e}^{-2\beta_0 y}+b\exp[-y(4\beta_0^2+2\omega_{\mathrm{I}}R_*)^{\frac{1}{2}}]. \tag{3.16}$$

If $(2\omega_I R_* + 4\beta_0^2)$ is positive, then the sign of the square root can be chosen to be positive so that $\tilde{V}_M$ vanishes at infinity. However, the argument of the square root at the resonant point is negative.

To obtain a solution $V_M(y,t)$ of (3.13), which vanishes at $y = \infty$, we solve it as an initial-value problem without assuming the exponential time dependence. Since it is not clear which initial condition for $V_M(y,t)$ is an appropriate one, it will be assumed that it vanishes initially and examine the y- and t-dependences of the resulting solution.

In order to solve the initial-value problem, the Laplace transform of (3.13) is taken to give

$$\left[is\left(\frac{\partial^2}{\partial y^2}-4\beta_0^2\right)-\frac{1}{R_*}\left(\frac{\partial^2}{\partial y^2}-4\beta_0^2\right)^2\right]\tilde{V}_M = -4BB^*\frac{\alpha_0^2\beta_0^2}{(\alpha_0^2+\beta_0^2)^2}\frac{\partial(\hat{\eta}_0\hat{\eta}_0^*)}{\partial y}\frac{1}{2\omega_I - is}, \quad (3.17)$$

where $\tilde{V}_M$ is the Laplace transform of V_M defined as

$$\tilde{V}_M(y,s) = \int_0^\infty dt\, e^{-ist} V_M(y,t). \quad (3.18)$$

The above equation for $\tilde{V}_M$ is solved using the Green function technique. The Green function takes the following form:

$$G = \begin{cases} A_+ \exp\left[(y-y_0)(4\beta_0^2+iR_*s)^{\frac{1}{2}}\right] + B_+ e^{-2\beta_0(y-y_0)} & \text{for } y > y_0, \\ A_- \exp\left[(y-y_0)(4\beta_0^2+iR_*s)^{\frac{1}{2}}\right] + B_- e^{-2\beta_0(y-y_0)} + C_- \exp\left[(y-y_0)(4\beta_0^2+iR_*s)^{\frac{1}{2}}\right] \\ \qquad + D_- e^{2\beta_0(y-y_0)} & \text{for } y < y_0, \end{cases} \quad (3.19)$$

where y_0 denotes the support of the delta function, and the coefficients $A_\pm$, $B_\pm$, C_- and D_- are determined from the boundary condition at the wall and the continuity of G, G' and G'' and the jump condition of G''' at $y = y_0$. Since $\tilde{V}_M$ does not have a homogeneous solution, the Green function is uniquely defined by these conditions. The branch cut associated with the square root is chosen as in figure 4.

The function $V_M(y,t)$ is then computed by taking the inverse Laplace transform where the integration contour in the complex s-plane should lie below all the poles and the branch cut of the integrand. Note that the pole associated with the source term is located on the branch cut since $R_* > 2\beta_0^2/|\omega_I|$. Further, the singularities in the expressions for the coefficients $A_\pm$, etc. are removable. Therefore, the contour can be deformed to a branch-cut integral. For the integration along the branch cut and for the integration over y_0, we have to rely on numerical evaluation. Figure 5(*b*) shows the results. Note that the y-dependence of $V_M(y,t)$ does not change very much with time. The amplitude of V_M reaches its maximum value at $t^+ = tu_\tau/\nu = 40$ and then decays very slowly compared with the source term's decay rate. (Recall that the source term of (3.13) decays as $\exp(-0.074\, t^+)$; in contrast, the value of V_M at $t^+ = 200$ is still about $\frac{1}{3}$ of its peak.)

To obtain the horizontal components of the induced mean flow, (3.5) is examined up to the order of $\epsilon^{\frac{1}{2}}$. Using (3.10) for $U^{(0)}$ and $W^{(0)}$, and (3.12) for $V^{(0)}$, the equation for $N^{(\frac{1}{2})}$ can be simplified to

$$\left[\left(\frac{\partial}{\partial t}+\bar{u}\frac{\partial}{\partial x}\right)-\frac{1}{R_*}\Delta\right]N^{(\frac{1}{2})} = 2\beta_0\bar{u}' V_M \sin(2\beta_0 z). \quad (3.20)$$

As for the computation for V_M, a solution is sought of the form

$$N^{(\frac{1}{2})} = N_M(y,t)\sin(2\beta_0 z). \quad (3.21)$$

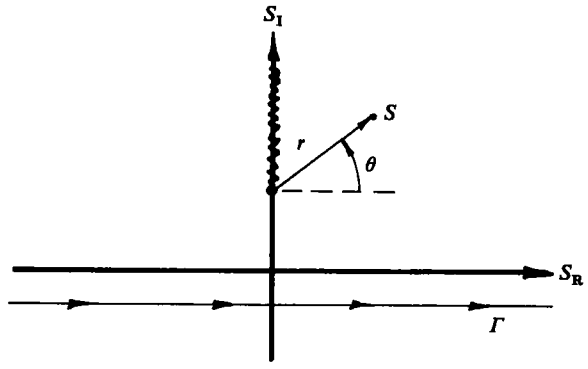

FIGURE 4. Branch cut of $(4\beta_0^2+\mathrm{i}R_*S)^{\frac{1}{2}}$ and integration contour Γ. $(4\beta_0^2+\mathrm{i}R_*S)^{\frac{1}{2}}$ is defined by $R_*^{\frac{1}{2}}r\exp\mathrm{i}(\frac{1}{2}\theta+\frac{1}{4}\pi)$ where θ varies from $(-\frac{3}{2}\pi)$ to $(\frac{1}{2}\pi)$.

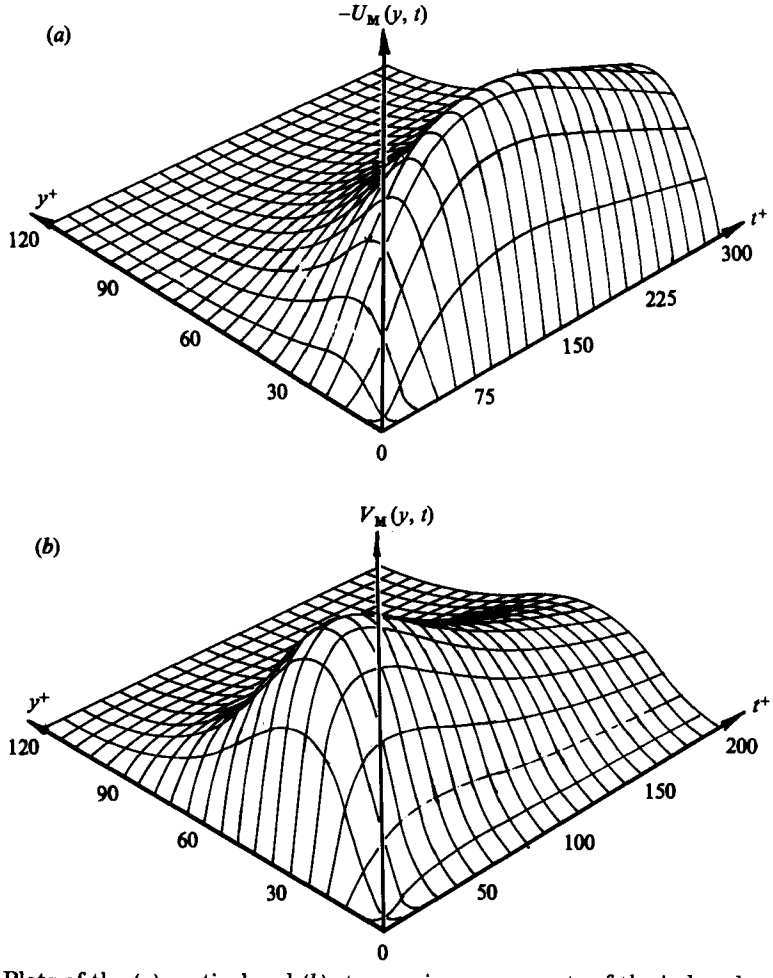

FIGURE 5. Plots of the (*a*) vertical and (*b*) streamwise components of the induced mean flow. The maximum of $|U_M(y,t)|$ is about 43% of the maximum of $V_M(y,t)$.

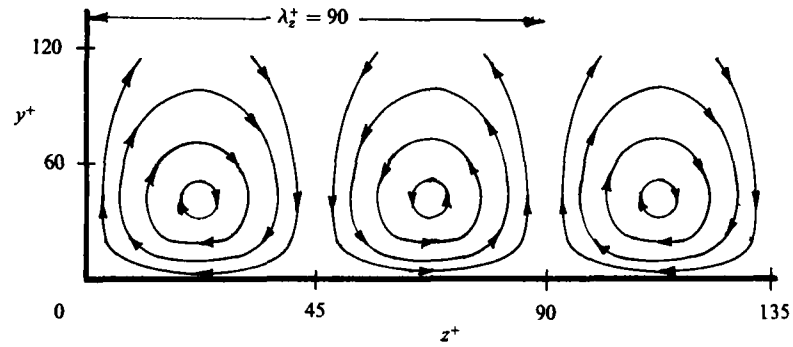

FIGURE 6. Computer streamline pattern of the induced mean flow at $t^+ = 40$. This pattern does not change for other values of t^+ as can be inferred from figure 5.

The resulting equation for $N_M(y,t)$ is solved again as an initial-value problem assuming that N_M vanishes initially. Using the Laplace transform and the Green-function technique, the computation of N_M can also be reduced to an evaluation of an integral over y_0 and over a contour in the frequency domain. Once N_M is computed, the horizontal components of the induced mean flow are obtained using the continuity equation and the definition of the vertical vorticity.

To summarize, the induced mean flow is given by

$$\left.\begin{aligned} U_M &= U_M(y,t)\cos(2\beta_0 z), \\ V_M &= V_M(y,t)\cos(2\beta_0 z) \\ W_M &= -(2\beta_0)^{-1}\frac{\partial V_M}{\partial y}\sin(2\beta_0 z), \end{aligned}\right\} \tag{3.22}$$

where U_M is related to N_M by

$$U_M = -\frac{N_M}{2\beta_0}. \tag{3.23}$$

The y,t dependence of U_M is plotted in figure 5(*a*). As for the vertical component of the induced mean flow, the y-dependence of U_M is rather independent of time. The amplitude of U_M reaches its maximum value at $t^+ = 150$ and then decays very slowly with time. In order to interpret the results plotted in figure 5, it is helpful to plot the projection, on the (y,z)-plane, of the streamlines. Figure 6 shows the streamline pattern at $t^+ = 40$. Actually, since the y-dependence of V_M does not change very much with time, the streamline pattern is about the same for all time. The streamline pattern clearly shows the counter-rotating longitudinal vortex structure of the induced mean flow. The spanwise wavelength λ_z^+ of the induced mean flow is 90, which compares favourably with the experimental value of 100.

At $z^+ = 0$, the counter-rotating vortices pump the low-speed fluid up away from the wall so that the streamwise component of the induced mean flow would show a momentum defect. These low-speed streaks would occur every 90 wall units in the spanwise direction.

In figure 7, the y-dependence of the computed vortex structure with accompanying low-speed streaks is compared with the vortex structure determined by Kim's (1983) numerical simulation. Only the shape is compared since the absolute values are not available in our analysis and the relative strengths of $\langle V\rangle_{max}$ and $\langle U\rangle_{max}$ are not

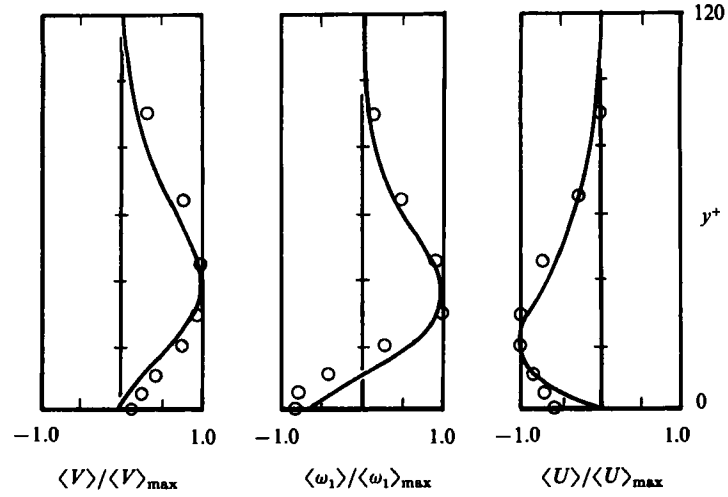

FIGURE 7. Comparison of the computed vortex structure with that of Kim (1983). The solid lines represent the analysis result and the circles represent Kim's result at $x^+ = 125$, where $x^+ = 0$ corresponds to the burst detection point. ω_1 denotes the streamwise vorticity.

available in Kim's paper. The similarity of our computed vortex shape with Kim's simulation supports the relevance of the resonance mechanism to the bursting phenomena. The agreement between Kim's simulation results and Blackwelder & Kaplan's experimental results is generally good if the slight differences are attributed to the difference between temporal and spatial averaging.

4. Concluding remarks

It is natural to be concerned with the robustness of the direct resonance and for this reason the effect on resonant conditions of different boundary conditions, mean profiles, and with eddy-viscosity terms in the equation were examined. As mentioned in §2, replacing the quasi-laminar model with the Newtonian eddy model does not affect the existence of a direct resonance and the computed induced mean flow exhibits features similar to those described in §3. With the mean profile observed by Reischman & Tiderman (1975) for a polymer-injected turbulent boundary layer, the direct resonance was still found to remain. The spanwise wavenumber at the resonance is, however, smaller than that for the 'universal' mean profile, which agrees with experimental evidence of the wider streak spacing for a polymer-added flow. We also confirmed that direct resonance is virtually unaffected even if we replace the rigid wall with a compliant wall.

There are, of course, several aspects of the present theory that remain incomplete. However, this study provides strong evidence for the relevance of direct resonance to the appearance of streamwise vortices observed in a turbulent boundary layer. In terms of the energy exchange between the mean flow and the fluctuations, direct resonance can be interpreted as follows: the source term in the linearized vertical-vorticity equation (2.16) reflects the production of horizontal disturbance energy by the action of the mean field $\overline{u}$ against the uv-component of the Reynold's stresses. When the wavenumbers and the frequency associated with the Orr–Sommerfeld eigenmode correspond to those of a free mode of the vertical vorticity, the production of energy through the uv-Reynolds stress becomes more efficient. This situation is

similar to the harmonic oscillator driven by broadband noise about its natural frequency.

We found two main pieces of evidence for the relevance of such a mechanism to the bursting process. One is that the wavenumbers and frequency at resonance are close to the values associated with the most-intense waves measured by Morrison & Kronauer near the sublayer boundary. The other is that the secondary mean flow induced by this resonant fundamental mode contains a streamwise vortex structure. The theoretical shape of the vortices and the spacing of the accompanying low-speed streaks are comparable with experimental findings.

One of the problems which has not been addressed is a comparison of the resonant point and other points in wavenumber space. In order to extend the theory to predict the power-spectral distribution, this issue has to be addressed. A difficulty associated with this extension is that although the resonant mode initially grows with time, the exponentially decaying factor eventually dominates and the mode decays. Therefore, without a fresh supply of disturbances, this resonance cannot sustain itself. In this respect, a potentially important property of this resonant mode seems to be the inflexional instability. As a test, we considered a one-parameter family of mean profiles which starts with the universal mean profile at $s = 0$ and ends with the inflexional profile found by Blackwelder & Kaplan at $s = 1$ (i.e. $u_s(y) = (1-s)u(y)+su_{\mathrm{BK}}$, where u_{BK} denotes the Blackwelder & Kaplan profile. As s increases, the damping factor associated with the Orr–Sommerfeld mode becomes smaller and near $s = 0.7$ that mode becomes unstable. As it becomes unstable, it can no longer resonate with the vertical vorticity mode since it can be shown analytically that all the free vertical vorticity modes are damped. Although at $s = 0$ the resonant Orr–Sommerfeld mode is not the least-damped mode (actually it is the second least-damped mode; the eigenfrequency of the least-damped mode being $\omega^+ = 0.13+0.035\mathrm{i}$ at α^+ and β^+ given by (2.24) and (2.25)), as s increases this order in damping factor changes and only the resonant mode becomes unstable at $s = 1$. These two properties of the second mode (when ordered by the imaginary part of the eigenfrequency), i.e. the direct resonance and the inflexional instability, might be the reasons why it plays an important role even if it has a slightly larger damping factor. However, to estimate these effects quantitatively appears to require a more systematic account of the several lowest modes with varying wavenumbers.

Another problem which has not been considered concerns the origin and mathematical description of the sweep. This might involve a very complicated interaction between the outer flow and the near-wall flow. In this regard, it seems appropriate to mention that the induced mean flow in §3 was represented by an integral along a branch cut in the complex frequency plane. This branch cut is what Mack (1976) interpreted as the continuous spectrum. For a frequency in this continuous spectrum, the corresponding eigensolution does not decay exponentially but becomes oscillatory as y approaches infinity. This raises a possibility that the interaction between the inner and the outer flows could be described through the induced mean flow. Recall that the initial condition for the induced mean flow was chosen to be zero in §3 since we do not know what an appropriate condition should be. Perhaps by choosing an initial condition as appropriate to a finite wavepacket rather than an infinite plane wave, the time development of the induced mean flow would exhibit characteristics of the sweep in addition to the vortex structure.

This research was sponsored by the Office of Naval Research under Contract N00014-81-C-0440. The technical monitors for this research were M. Reischman (at

ONR) and J. Hanson (at NRL). The authors acknowledge the valuable suggestions and comments of T. Kubota and Y. M. Chen, as well as M. Reischman and J. Hanson. We also thank Y. M. Chen and M. Goforth for their assistance in the numerical computations.

REFERENCES

BARK, F. H. 1975 *J. Fluid Mech.* **70**, 229.

BENNEY, D. J. 1961 *J. Fluid Mech.* **10**, 209.

BENNEY, D. J. 1984 *Stud. Appl. Math.* **70**, 1.

BENNEY, D. J. & GUSTAVSSON, L. H. 1981 *Stud. Appl. Math.* **64**, 185.

BLACKWELDER, R. F. 1979 In *Coherent Structures of Turbulent Boundary Layers* (ed. C. R. Smith & D. E. Abbott), p. 211. Lehigh University.

BLACKWELDER, R. F. 1983 *Phys. Fluids* **26**, 2807.

BLACKWELDER, R. F. & KAPLAN, R. E. 1976 *J. Fluid Mech.* **76**, 89.

CANTWELL, B. J. 1981 *Ann. Rev. Fluid Mech.* **13**, 457.

COLES, D. 1979 In *Coherent Structures of Turbulent Boundary Layers* (ed. C. R. Smith & D. E. Abbott), p. 462. Lehigh University.

CORINO, E. R. & BRODKEY, R. S. 1969 *J. Fluid Mech.* **37**, 1.

KIM, J. 1983 *Phys. Fluids* **26**, 2088.

KLEBANOFF, P. D., TIDSTROM, D. & SARGENT, L. M. 1962 *J. Fluid Mech.* **12**, 1.

KLINE, S. J., REYNOLDS, W. D., SCHRAUB, J. A. & RENSTADLER, P. W. 1967 *J. Fluid Mech.* **30**, 74.

LANDAHL, M. T. 1967 *J. Fluid Mech.* **29**, 441.

LIN, C. C. & BENNEY, D. J. 1962 *Am. Math. Soc., Proc. Symp. Appl. Math.* **13**, 1.

MACK, L. M. 1976 *J. Fluid Mech.* **73**, 497.

MORRISON, W. R. B. & KRONAUER, R. E. 1969 *J. Fluid Mech.* **39**, 117.

REISCHMAN, M. M. & TIDERMAN, W. G. 1975 *J. Fluid Mech.* **70**, 369.

REYNOLDS, W. C. & HUSSAIN, A. K. M. F. 1972 *J. Fluid Mech.* **54**, 263.

STUART, J. T. 1967 *J. Fluid Mech.* **29**, 417.

WALLACE, J. W., BRODKEY, R. S. & ECKELMANN, H. 1977 *J. Fluid Mech.* **83**, 673.